Tunable emission from silico-carnotite type double silicates doped with Tb^{3+} and Eu^{3+}

I. Carrasco,* F. Piccinelli, and M. Bettinelli

Luminescent Materials Laboratory, Department of Biotechnology, University of Verona, 37134 Verona, Italy
* *irene.carrascoruiz@univr.it*

Abstract: Double silicates with the silico-carnotite orthorhombic structure and co-doped with Tb^{3+} and Eu^{3+} have been prepared by solid-state reaction. Room temperature luminescence spectra and decay kinetics have been measured and analysed. Upon UV excitation at 378 nm, the emission colour varies from red to pinkish, depending on the doping level. The resulting colour can be adjusted by controlling the Tb^{3+}/Eu^{3+} concentration ratio. Control of the doping leads to close-to-white emission in some of the analysed samples upon excitation in the wavelength region useful for LED lighting.

OCIS codes: (160.2540) Fluorescent and luminescent materials; (160.5690) Rare-earth-doped materials; (300.6280) Spectroscopy, fluorescence and luminescence; (300.6550) Spectroscopy, visible.

References and links

1. European Commission, Green Paper Lighting the Future: Accelerating the deployment of innovative lighting technologies (2011).
2. C. C. Lin and R.-S. Liu, "Advances in phosphors for light-emitting diodes," J. Phys. Chem. Lett. **2**(11), 1268–1277 (2011).
3. P. P. Pawar, S. R. Munishwar, and R. S. Gedam, "Physical and optical properties of Dy^{3+}/Pr^{3+} Co-doped lithium borate glasses for W-LED," Alloys and Comp. **660**, 347–355 (2016).
4. H. Guo, H. Zhang, J. Li, and F. Li, "Blue-white-green tunable luminescence from $Ba_2Gd_2Si_4O_{13}:Ce^{3+},Tb^{3+}$ phosphors excited by ultraviolet light," Opt. Express **18**(26), 27257–27262 (2010).
5. Y. Liu, X. Zhang, Z. Hao, X. Wang, and J. Zhang, "Tunable full-color-emitting $Ca_3Sc_2Si_3O_{12}:Ce^{3+}$, Mn^{2+} phosphor via charge compensation and energy transfer," Chem. Commun. (Camb.) **47**(38), 10677–10679 (2011).
6. Y. Liu, J. Zhang, C. Zhang, J. Jiang, and H. Jiang, "High efficiency green phosphor $Ba_9Lu_2Si_6O_{24}:Tb^{3+}$: visible quantum cutting via cross-relaxation energy transfers," J. Phys. Chem. C **120**(4), 2362–2370 (2016).
7. F. Piccinelli, A. Speghini, G. Mariotto, L. Bovo, and M. Bettinelli, "Visible luminescence of lanthanide ions in $Ca_3Sc_2Si_3O_{12}$ and $Ca_3Y_2Si_3O_{12}$," J. Rare Earths **27**(4), 555–559 (2009).
8. F. Piccinelli, A. Lausi, and M. Bettinelli, "Structural investigation of the new $Ca_3Ln_2Ge_3O_{12}$ (Ln=Pr, Nd, Sm, Gd and Dy) compounds and luminescence spectroscopy of $Ca_3Gd_2Ge_3O_{12}$ doped with the Eu^{3+} ion," J. Solid State Chem. **205**, 190–196 (2013).
9. I. Carrasco, K. Bartosiewicz, M. Nikl, F. Piccinelli, and M. Bettinelli, "Energy transfer processes in $Ca_3Tb_{2-x}Eu_xSi_3O_{12}$(x= 0–2)," Opt. Mater. **48**, 252–257 (2015).
10. B. Dickens and W. E. Brown, "Crystal structure of $Ca_3(PO_4)_2SiO_4$ (silico-carnotite)," Tschermaks Mineral. Petrogr. Mitt. **16**(1-2), 1–27 (1971).
11. G. A. Novak and G. V. Gibbs, "The crystal chemistry of the silicate garnets," Am. Mineral. **56**, 791–825 (1971).
12. F. Piccinelli, A. Lausi, A. Speghini, and M. Bettinelli, "Crystal structure study of new lanthanide silicates with silico-carnotite structure," J. Solid State Chem. **194**, 233–237 (2012).
13. F. Auzel, J. Dexpert-Ghys, D. Morin, G. Dadoun, J. Ostorero, and H. Makram, "Strong self-quenching of Tb^{3+} in two stoichiometric materials: ultraphosphate and chloroapatite," Mater. Res. Bull. **16**(12), 1521–1525 (1981).
14. J. F. M. dos Santos, I. A. A. Terra, N. G. C. Astrath, F. B. Guimaraes, M. L. Baesso, L. A. O. Nunes, and T. Catunda, "Mechanisms of optical losses in the $^5D_4$ and $^5D_3$ levels in Tb^{3+} doped low silica calcium aluminosilicate glasses," J. Appl. Phys. **117**(5), 053102 (2015).
15. Z. Hao, J. Shang, X. Zhang, S. Lu, and Z. Wang, "Blue-green-emitting phosphors $CaSc_2O_4:Tb^{3+}$: Tunable luminescence manipulated by cross-relaxation," J. Electr. Soc. **156**(3), H193–H196 (2009).
16. F. Piccinelli, A. Speghini, and M. Bettinelli, "Crystal structure and optical spectroscopy of $Ca_3Ln_2Si_3O_{12}$ (Ln= Gd and Lu) doped with Eu^{3+}," Opt. Mater. **35**(11), 2027–2029 (2013).
17. M. Bettinelli, F. Piccinelli, A. Speghini, J. Ueda, and S. Tanabe, "Excited state dynamics and energy transfer rates in $Sr_3Tb_{0.90}Eu_{0.10}(PO_4)_3$," J. Lumin. **132**(1), 27–29 (2012).

#258303 Received 26 Jan 2016; revised 11 Apr 2016; accepted 11 Apr 2016; published 28 Apr 2016

18. T. Hoshina, "Radiative transition probabilities in Tb^{3+} and fluorescence colors producible by Tb^{3+}-activated phosphors," Jpn. J. Appl. Phys. **6**(10), 1203–1211 (1967).

1. Introduction

Due to the increased demand of lighting worldwide, new energy efficient and environmentally friendly lighting devices are strongly required. Solid state lighting systems are gradually replacing the old technologies thanks to their excellent stability, fast response, longer life expectancy, environmentally friendly characteristics and high luminous efficiency [1, 2].

White light can be produced by the combination of the fundamental colours (red, green and blue) coming from three individual LEDs, or combining only one LED with suitable phosphors. For this second approach, commercially available blue and near ultraviolet (NUV) LEDs can be used to excite either a yellow phosphor or a green and red phosphor (using blue LEDs), or to excite blue, green and red phosphors (using NUV LEDs) [2]. Both approaches offer the production of white-LEDs with comparable brightness. Nevertheless, in the three converter system, the blue emission efficiency is low due to strong re-absorption of the blue light. As a consequence, the development of novel single-phased white-emitting phosphors is attracting a lot of attention over the last years [2–5].

Inorganic phosphors doped with rare earth ions have drawn much interest because of their intense emission efficiencies due to *4f-4f* and *4f-5d* electronic transitions, and are currently used in many technological fields. Silicate phosphors present high interest from the spectroscopic point of view due to their good transparency in the UV/VIS region and chemical stability, and are to be considered as efficient hosts for doping with luminescent trivalent lanthanide ions [6, 7].

In this paper, the room temperature luminescence spectra and decay kinetics of $Ca_3A_{1.98}Tb_{0.02}Si_3O_{12}$ (A = Gd, Y), $Ca_3A_{1.98}Eu_{0.02}Si_3O_{12}$ (A = Gd, Y), $Ca_3Gd_{2-x-y}Tb_xEu_ySi_3O_{12}$ and $Ca_3Y_{2-x-y}Tb_xEu_ySi_3O_{12}$ phosphors belonging to silico-carnotite family have been systematically studied for various Tb^{3+} and Eu^{3+} doping concentration, upon UV excitation.

2. Experimental methods and structural characterization

Polycrystalline samples of $Ca_3A_{1.98}Tb_{0.02}Si_3O_{12}$ (A = Gd, Y), $Ca_3A_{1.98}Eu_{0.02}Si_3O_{12}$ (A = Gd, Y), $Ca_3Gd_{2-x-y}Tb_xEu_ySi_3O_{12}$ (x = 0.02, y = 0.04; x = 0.02, y = 0.01; x = 0.01, y = 0.01 and x = 0.01, y = 0.005) and $Ca_3Y_{2-x-y}Tb_xEu_ySi_3O_{12}$ (x = 0.02, y = 0.005; x = 0.015, y = 0.003; and x = 0.01, y = 0.005) were prepared by solid state reaction at high temperature (1450 ° C), following the procedures previously described [8,9].

Powder X-ray diffraction (XRD) measurements were performed to analyze the structure of the synthesized compounds. Experiments were carried out with a Thermo ARL X'TRA powder diffractometer, operating in the Bragg-Brentano geometry and equipped with a Cu-anode X-ray source (Kα, λ = 1.5418 A), using a Peltier Si (Li) cooled solid state detector. The patterns were collected with a scan rate of 0.04°/s in the 5-90° 2θ range. The phase identification was performed with the PDF-4 + 2013 database provided by the International Centre for Diffraction Data (ICDD). Polycrystalline samples were ground in a mortar and then put in a low-background sample holder for the data collection. All the obtained materials are single phase. They are isostructural with silico-carnotite $Ca_5(PO_4)_2SiO_4$ (orthorhombic, space group, *Pnma*) [10]. The structural formula can be represented as $AB_2C_2(EO_4)_3$ where A, B and C refer, respectively, to nine-, eight-, and seven-coordinate cationic sites, characterized by very low site symmetries (C_1 or C_s). E could be Si, P or both. It has been shown previously that the $Ca_3RE_2Si_3O_{12}$ (RE-rare earth ions) family of compounds possess orthorhombic *Pnma* crystal structure, and the distribution of the cations on the three available crystal sites is strongly dependent on the nature of the rare earth ion [11,12].

Room temperature luminescence spectra and decay curves were measured with a Fluorolog 3 (Horiba-Jobin Yvon) spectrofluorometer, equipped with a Xe lamp, a double

#258303 Received 26 Jan 2016; revised 11 Apr 2016; accepted 11 Apr 2016; published 28 Apr 2016

excitation monochromator, a single emission monochromator (mod.HR320) and a photomultiplier in photon counting mode for the detection of the emitted signal.

3. Results and discussion

3.1 $Ca_3Gd_{2-x-y}Tb_xEu_ySi_3O_{12}$

Figure 1(a) shows the room temperature emission spectra of $Ca_3Gd_{1.98}Tb_{0.02}Si_3O_{12}$ measured upon excitation at 377 nm (in $^5D_3$ level of Tb^{3+}) and of $Ca_3Gd_{1.98}Eu_{0.02}Si_3O_{12}$ recorded upon excitation at 393 nm. For $Ca_3Gd_{1.98}Tb_{0.02}Si_3O_{12}$ the emission presents various bands in the ranges 400-480 and 500-650 nm. These bands are due to the $^5D_3 \rightarrow {}^7F_J$ (J = 5, 4, 3) and $^5D_4 \rightarrow {}^7F_J$ (J = 6, 5, 4, 3) transitions. Among them, the $^5D_4 \rightarrow {}^7F_5$ green emission at 542 nm is the most intense.

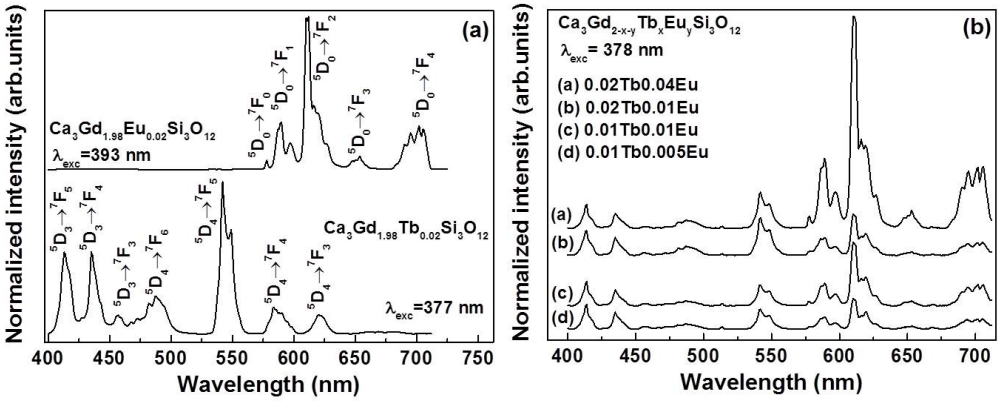

Fig. 1. (a) Room temperature emission spectra of $Ca_3Gd_{1.98}Tb_{0.02}Si_3O_{12}$ (λ_{exc} = 377 nm) and $Ca_3Gd_{1.98}Eu_{0.02}Si_3O_{12}$ (λ_{exc} = 393 nm). The spectra are normalized to Tb^{3+} $^5D_4 \rightarrow {}^7F_5$ emission, and Eu^{3+} $^5D_0 \rightarrow {}^7F_2$ emission respectively. (b) Room temperature emission spectra of $Ca_3Gd_{2-x-y}Tb_xEu_ySi_3O_{12}$ measured upon excitation at 378 nm. All spectra are normalized to Tb^{3+} $^5D_3 \rightarrow {}^7F_5$ emission.

As expected in diluted terbium materials, no quenching of the blue emission is observed. This is because the cross relaxation processes (CR) that transfer population from $^5D_3$ to $^5D_4$, are concentration dependent [13–15], and therefore they are not efficient at low terbium concentration levels. Taking into account that the vibrational cut-off of the $Ca_3Y_2Si_3O_{12}$ silico-carnotite host is about 1050 cm^{-1}, and the energy gap between $^5D_3$ and $^5D_4$ levels is about 5750 cm^{-1} [7], the gap can be bridged by 4-5 phonons. Since for the $Ca_3Gd_2Si_3O_{12}$ host similar vibrational cut-off values are expected, in this system it is possible to populate $^5D_4$ from $^5D_3$ by multiphonon relaxation (MPR). The presence of these processes explains the origin of the green emission bands observed in the spectrum measured upon $^5D_3$ excitation. In the case of $Ca_3Gd_{1.98}Eu_{0.02}Si_3O_{12}$ five bands in the 590 –730 nm range are observed upon excitation at 393 nm in the $^5L_6$ level. These emission bands correspond to the $^5D_0 \rightarrow {}^7F_J$ (J = 0, 1, 2, 3, 4) transitions of Eu^{3+}, the most intense being the hypersensitive $^5D_0 \rightarrow {}^7F_2$ red emission at 612 nm, as expected due to the distorted geometry of the sites accommodating the impurity [16].

In view of these results, it is interesting to consider the possibility of combining the blue, green and red emissions observed in the $Ca_3Gd_2Si_3O_{12}$ phosphors doped with Tb^{3+} and Eu^{3+}. In order to study this phenomenon, a series of $Ca_3Gd_{2-x-y}Tb_xEu_ySi_3O_{12}$ (x = 0.02, y = 0.04; x = 0.02, y = 0.01; x = 0.01, y = 0.01 and x = 0.01, y = 0.005) samples have been prepared. The excitation populates the $^5D_3$ and $^5L_7$ levels of Tb^{3+} and Eu^{3+}, respectively. The emission spectra of the powders (λ_{exc} = 378 nm) are presented in Fig. 1(b). The spectra present various emission bands originating from the $^5D_3$ and $^5D_4$ levels of Tb^{3+} (blue to yellow range), and

#258303 Received 26 Jan 2016; revised 11 Apr 2016; accepted 11 Apr 2016; published 28 Apr 2016

from the $^5D_0$ level of Eu^{3+} (orange to red range). It is observed that the relative intensities of the $^5D_3 \rightarrow {}^7F_J$ and $^5D_4 \rightarrow {}^7F_J$ transitions do not vary significantly when modifying Tb^{3+} concentration. This is because, as discussed before, the doping levels are low (from 1 to 0.5 mol%), so the non-radiative relaxation from $^5D_3$ to $^5D_4$ is not enhanced. The relative intensities of the blue/green bands respect to the red ones, however, are strongly affected by the Tb^{3+}/Eu^{3+} concentration ratio: it is observed that if the concentration of Tb^{3+} is equal or lower than the concentration of Eu^{3+}, the intensity of the red bands is almost double than for blue-green ones. On the contrary, if Tb^{3+} concentration is higher than Eu^{3+}, the relative intensities tend to be identical. Controlling the doping ratio thus allows changing the final emission colour of the material from red to pinkish-white. To clarify this point, the CIE XYZ chromaticity coordinate diagram is shown in Fig. 2. The calculated values of CIE coordinates are provided in Table 1. For completeness, CIE values for $Ca_3Gd_{1.98}Tb_{0.02}Si_3O_{12}$ and $Ca_3Gd_{1.98}Eu_{0.02}Si_3O_{12}$ are also included.

For all the compounds, the emission bands are relatively broad due to the structural disorder present in the host, as previously observed in other silico-carnotite materials doped with Tb^{3+} and Eu^{3+} [9].

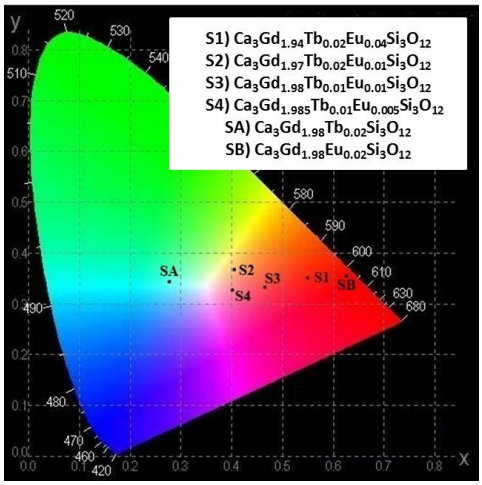

Fig. 2. CIE diagram coordinates of $Ca_3Gd_{1.98}Tb_{0.02}Si_3O_{12}$, $Ca_3Gd_{1.98}Tb_{0.02}Si_3O_{12}$ and $Ca_3Gd_{2-x-y}Tb_xEu_ySi_3O_{12}$ excited at 377, 378 and 393 nm respectively.

Table 1. Calculated values for CIE coordinates of $Ca_3Gd_{1.98}Tb_{0.02}Si_3O_{12}$ and $Ca_3Gd_{2-x-y}Tb_xEu_ySi_3O_{12}$ excited at 378 nm and $Ca_3Gd_{1.98}Eu_{0.02}Si_3O_{12}$ excited at 393 nm.

Material	x	y
$Ca_3Gd_{1.98}Tb_{0.02}Si_3O_{12}$	0.2661	0.3240
$Ca_3Gd_{1.98}Eu_{0.02}Si_3O_{12}$	0.6303	0.3582
$Ca_3Gd_{1.94}Tb_{0.02}Eu_{0.04}Si_3O_{12}$	0.5502	0.3631
$Ca_3Gd_{1.97}Tb_{0.02}Eu_{0.01}Si_3O_{12}$	0.4133	0.3738
$Ca_3Gd_{1.98}Tb_{0.01}Eu_{0.01}Si_3O_{12}$	0.4725	0.3448
$Ca_3Gd_{1.985}Tb_{0.01}Eu_{0.005}Si_3O_{12}$	0.4057	0.3300

The excitation spectra of all samples are shown in Fig. 3. The spectrum of $Ca_3Gd_{1.98}Tb_{0.02}Si_3O_{12}$ is composed of overlapping bands in the UV ranging from 300 nm to almost 400 nm, and a band at 480 nm. The transitions have been assigned as $^7F_6 \rightarrow {}^5G_3$ at 340 nm, $^7F_6 \rightarrow {}^5L_8 + {}^5G_4$ at 350 nm, $^7F_6 \rightarrow {}^5D_3$ at377 nm and $^7F_6 \rightarrow {}^5D_4$ at 480 nm. For the $Ca_3Gd_{2-x-y}Tb_xEu_ySi_3O_{12}$ phosphors, the excitation spectra when monitoring the emission of Tb^{3+} (λ_{emi} = 542 nm) are composed of the same bands observed for $Ca_3Gd_{1.98}Tb_{0.02}Si_3O_{12}$. In the case of the samples with less Tb^{3+} doping, it is possible to observe that the intensity of the $^7F_6 \rightarrow {}^5D_4$ band is comparable to the $^7F_6 \rightarrow {}^5D_3$ band.

#258303 Received 26 Jan 2016; revised 11 Apr 2016; accepted 11 Apr 2016; published 28 Apr 2016

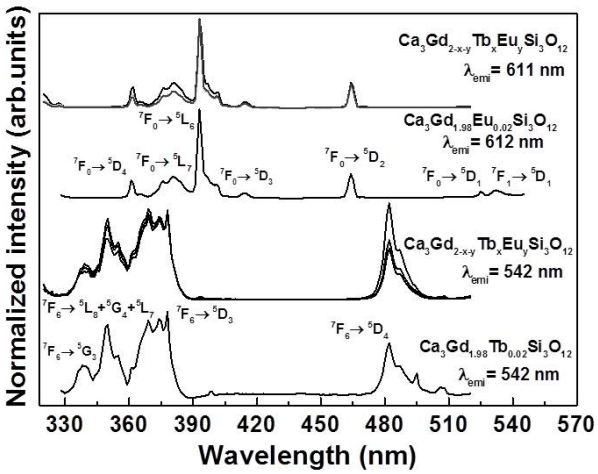

Fig. 3. (a) Room temperature excitation spectra of $Ca_3Gd_{1.98}Tb_{0.02}Si_3O_{12}$ (λ_{emi} = 542 nm), $Ca_3Gd_{1.98}Eu_{0.02}Si_3O_{12}$ (λ_{emi} = 612 nm) and $Ca_3Gd_{2-x-y}Tb_xEu_ySi_3O_{12}$ monitoring both emission of Tb^{3+} and Eu^{3+} (λ_{emi} = 542 nm, and λ_{emi} = 611 nm). The spectra are normalized to Tb^{3+} $^7F_6 \rightarrow {}^5D_3$ band, and Eu^{3+} $^7F_0 \rightarrow {}^5D_3$ band respectively.

The spectrum of $Ca_3Gd_{1.98}Eu_{0.02}Si_3O_{12}$ is composed of various bands ranging from 360 nm to 430 nm and other bands at 460 nm and 530 nm. In this case the transitions have been assigned as $^7F_0 \rightarrow {}^5D_4$ at 360 nm, $^7F_0 \rightarrow {}^5L_7$ at 393 nm, which it is the most intense, $^7F_0 \rightarrow {}^5D_3$ at 412 nm, $^7F_0 \rightarrow {}^5D_2$ at 460 nm and $^7F_0 \rightarrow {}^5D_1$ at 525 nm and $^7F_1 \rightarrow {}^5D_1$ at 530 nm. In the case of the co-doped samples, the excitation spectra when monitoring the emission of Eu^{3+} (λ_{emi} = 611 nm) present no differences respect to one the observed for $Ca_3Gd_{1.98}Eu_{0.02}Si_3O_{12}$. No evidence of Tb^{3+}-Eu^{3+} energy transfer is found in the spectra of these materials. This can be explained on the basis of the fact that in the co-doped systems the Tb^{3+} and the Eu^{3+} concentrations are low, and then the average distance between Ln^{3+} ions is estimated to lie between 10 and 16 Å, which is larger than the typical critical distance required for electric dipole-electric dipole energy transfer processes involving Tb^{3+} and Eu^{3+} (<10 Å) [17]. Moreover, this implies that there is no fast migration among Tb^{3+} ions. We have reported that in silico-carnotite materials, the energy migration in the Tb^{3+} subset plays a relevant role in the Tb^{3+}-Eu^{3+} energy transfer process [9]. Since in the present case Tb^{3+}-Tb^{3+} energy migration is not efficient, the absence of Tb^{3+}-Eu^{3+} energy transfer can be also expected.

Decay curves for Tb^{3+} and Eu^{3+} emission were measured upon excitation at 378 nm. Figure 4(a) shows decay curves for Tb^{3+} emission from $^5D_4$ in the various co-doped phosphors (diluted compounds). All the curves are plotted together. To compare the differences, a concentrated Tb^{3+} compound ($Ca_3Tb_2Si_3O_{12}$) is also included. The obtained time constants are reported in Table 2, together with the decay constant for $Ca_3Gd_{1.98}Tb_{0.02}Si_3O_{12}$. In the co-doped phosphors there is a clear rise at short times, which is not present in $Ca_3Tb_2Si_3O_{12}$. As reported in our previous work [9], this behaviour of $Ca_3Tb_2Si_3O_{12}$ is an effect of the high Tb^{3+} concentration, which allows easy $^5D_3 \rightarrow {}^5D_4$ cross relaxation in Tb^{3+} ions. As it was explained previously, in the co-doped materials there is no migration among Tb^{3+} ions and therefore the observed decay in this case is slow, as energy transfer to killer centres does not occur. The slow initial build up is due to the MPR processes involved in the population of $^5D_4$, that are slower than the CR processes that are present in $Ca_3Tb_2Si_3O_{12}$. Due to the low levels of doping, the shapes of the curves and the decay constants are not affected by Eu^{3+} concentration. This fact, together with the absence of energy migration in the Tb^{3+} subset and from Tb^{3+} to Eu^{3+}, explains why the decay curves present an almost identical behaviour in all the different $Ca_3Gd_{2-x-y}Tb_xEu_ySi_3O_{12}$ phosphors. As a result, the curves appear superimposed in the graph. The decay curves for Tb^{3+} emission from $^5D_3$ (blue bands) have been also

#258303 Received 26 Jan 2016; revised 11 Apr 2016; accepted 11 Apr 2016; published 28 Apr 2016

measured for $Ca_3Gd_{1.98}Tb_{0.02}Si_3O_{12}$ and the co-doped phosphors. The curves are not exponential due to the presence of structural disorder. Decay constant is in practice not affected by changes in Eu^{3+} concentration, and its value is about 1 ms for all the samples.

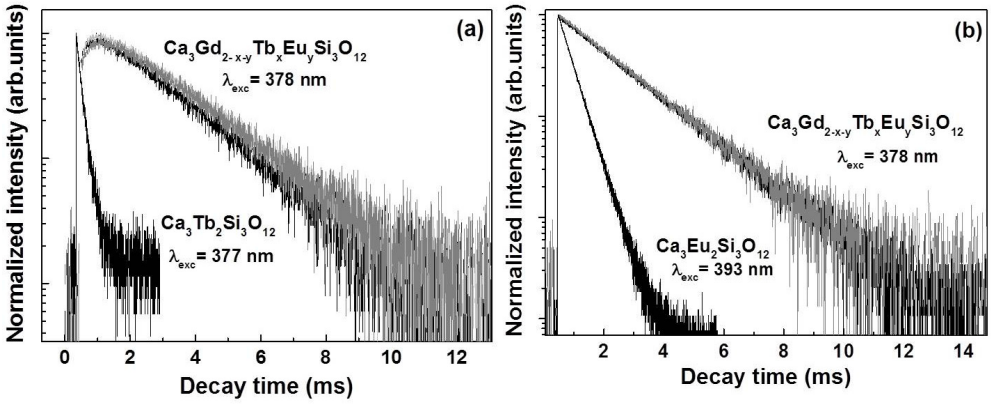

Fig. 4. (a) Room temperature decay curves of the $^5D_4$ Tb^{3+} emission excited at 377 nm ($Ca_3Tb_2Si_3O_{12}$) and at 378 nm ($Ca_3Gd_{2-x-y}Tb_xEu_ySi_3O_{12}$). (b) Room temperature decay curves of the $^5D_0$ Eu^{3+} emission excited at 378 nm ($Ca_3Gd_{2-x-y}Tb_xEu_ySi_3O_{12}$) and 393 nm ($Ca_3Eu_2Si_3O_{12}$).

Figure 4(b) presents the decay curves for Eu^{3+} $^5D_0$ emission for the various co-doped samples. All the curves are plotted together. $Ca_3Eu_2Si_3O_{12}$ is also included to compare the behaviour of the ion. The time constants calculated from the decay curves are also reported in Table 2. For the Eu^{3+}-doped samples, the curves are well fitted by a single exponential function. This behaviour is explained because there is no energy transfer from Tb^{3+} to Eu^{3+}, and thanks to the fast relaxation from the excited level ($^5L_6$ for the diluted compounds, $^5L_7$ for the concentrated sample) to $^5D_0$ due to the small energy gaps between the intermediate levels, which require less than three phonons to be bridged. In the case of $Ca_3Eu_2Si_3O_{12}$, decay time is shortened, presumably due to concentration quenching as a result of energy migration to quenching impurities. No significant changes are observed when varying Eu^{3+} concentration in the diluted samples. All the curves present an almost identical behaviour, and therefore they appear superimposed in the graph.

Table 2. Decay data for the luminescent levels of Tb^{3+} and Eu^{3+} in several oxide hosts upon UV excitation

Material	Excited state	Decay time (ms)	Excited state	Decay time (ms)
$Ca_3Tb_2Si_3O_{12}$	$^5D_4$ (Tb^{3+})	0.18	--	--
$Ca_3Eu_2Si_3O_{12}$	--	--	$^5D_0$ (Eu^{3+})	0.44
$Ca_3Gd_{1.98}Tb_{0.02}Si_3O_{12}$	$^5D_4$ (Tb^{3+})	2.32 rise + decay	--	--
$Ca_3Gd_{1.98}Eu_{0.02}Si_3O_{12}$	--	--	$^5D_0$ (Eu^{3+})	1.79
$Ca_3Gd_{1.94}Tb_{0.02}Eu_{0.04}Si_3O_{12}$	$^5D_4$ (Tb^{3+})	2.09 rise + decay	$^5D_0$ (Eu^{3+})	1.85
$Ca_3Gd_{1.94}Tb_{0.02}Eu_{0.01}Si_3O_{12}$	$^5D_4$ (Tb^{3+})	2.19 rise + decay	$^5D_0$ (Eu^{3+})	1.85
$Ca_3Gd_{1.94}Tb_{0.01}Eu_{0.01}Si_3O_{12}$	$^5D_4$ (Tb^{3+})	2.25 rise + decay	$^5D_0$ (Eu^{3+})	1.78
$Ca_3Gd_{1.94}Tb_{0.02}Eu_{0.005}Si_3O_{12}$	$^5D_4$ (Tb^{3+})	2.06 rise + decay	$^5D_0$ (Eu^{3+})	1.80

3.2 $Ca_3Y_{2-x-y}Tb_xEu_ySi_3O_{12}$

Due to the interesting properties observed for the gadolinium-based phosphors, it is worth to explore other similar hosts starting from these results. In the present section the luminescence of various yttrium-based silico-carnotite are discussed.

Figure 5(a) shows the room temperature emission spectra of $Ca_3Y_{1.98}Tb_{0.02}Si_3O_{12}$ measured upon excitation at 378 nm (in $^5D_3$ level of Tb^{3+}) and the emission spectrum of $Ca_3Y_{1.98}Eu_{0.02}Si_3O_{12}$ recorded upon excitation at 393 nm. In both cases, the spectra are similar to the ones presented in the previous section for the gadolinium-based samples. In the case of $Ca_3Y_{1.98}Tb_{0.02}Si_3O_{12}$, the emission spectrum presents various bands in the ranges of 400-480

#258303 Received 26 Jan 2016; revised 11 Apr 2016; accepted 11 Apr 2016; published 28 Apr 2016

and 500-650 nm, the most intense being the $^5D_4 \rightarrow {}^7F_5$ green emission at 542 nm. These results include the blue emission originating from the $^5D_3$ level, which was erroneously not shown and discussed in [7] published by some of us. In the case of $Ca_3Y_{1.98}Eu_{0.02}Si_3O_{12}$ five bands in the 590-730 nm range are observed. The most intense is the $^5D_0 \rightarrow {}^7F_2$ red emission at 612 nm. The changes of the structure due to the presence of one metal cation or another, *i.e.* the difference in the site distribution of Ca^{2+} and Ln^{3+} (including the luminescent dopant ones), lead to small differences of the average crystal field of the cations in each material [18]. These variations are responsible for the little changes observed in the blue/green (B/G) and orange/red (O/R) ratios of Tb^{3+} and Eu^{3+} emissions respectively, thus affecting the emission colour of the material. In Table 3 the B/G and O/R ratios calculated from the spectra for both gadolinium and yttrium-based compounds are presented.

Starting from the results obtained for the gadolinium silico-carnotite, a series of $Ca_3Y_{2-x-y}Tb_xEu_ySi_3O_{12}$ (x = 0.02, y = 0.005; x = 0.015, y = 0.003 and x = 0.01, y = 0.005) samples have been prepared. The emission spectra of the powders (λ_{exc} = 378 nm) are presented in Fig. 5(b). As it was observed for the gadolinium-based phosphors, the spectra present emission bands originating from the $^5D_3$ and $^5D_4$ levels of Tb^{3+} (blue to yellow range), and from the $^5D_0$ level of Eu^{3+} (orange to red range).

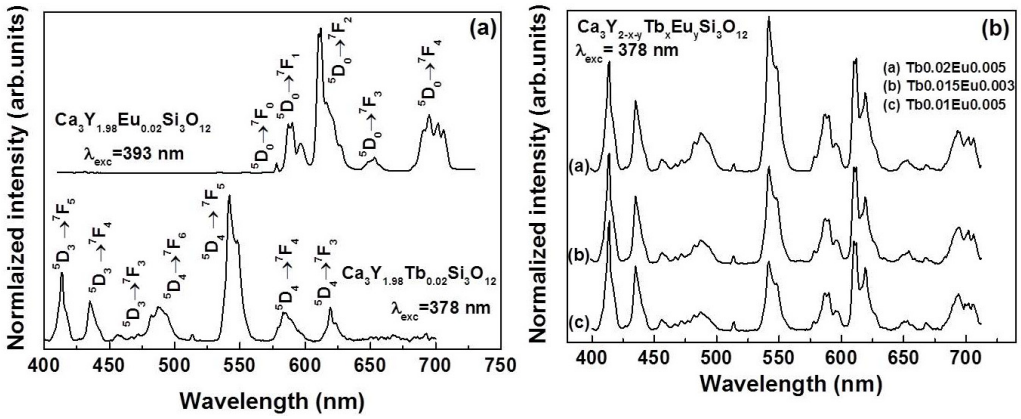

Fig. 5. (a) Room temperature emission spectra of $Ca_3Y_{1.98}Tb_{0.02}Si_3O_{12}$ (λ_{exc} = 377 nm) and $Ca_3Y_{1.98}Eu_{0.02}Si_3O_{12}$ (λ_{exc} = 393 nm). The spectra are normalized to Tb^{3+} $^5D_4 \rightarrow {}^7F_5$ emission, and Eu^{3+} $^5D_0 \rightarrow {}^7F_2$ emission respectively. (b) Room temperature emission spectra of $Ca_3Y_{2-x-y}Tb_xEu_ySi_3O_{12}$ measured upon excitation at 378 nm. All spectra are normalized to Tb^{3+} $^5D_3 \rightarrow {}^7F_5$ emission.

Table 3. Calculated values for B/G and O/R ratios for the $Ca_3A_{1.98}Tb_{0.02}Si_3O_{12}$ (A = Gd, Y), $Ca_3A_{1.98}Eu_{0.02}Si_3O_{12}$ (A = Gd, Y) phosphors.

Material	B/G ratio	O/R ratio
$Ca_3Gd_{1.98}Tb_{0.02}Si_3O_{12}$	1.69	–
$Ca_3Gd_{1.98}Eu_{0.02}Si_3O_{12}$	–	0.54
$Ca_3Y_{1.98}Tb_{0.02}Si_3O_{12}$	0.91	–
$Ca_3Y_{1.98}Eu_{0.02}Si_3O_{12}$	–	0.36

The CIE XYZ chromaticity coordinates diagram is shown in Fig. 6. The calculated values of CIE coordinates are reported in Table 4. As done before and for completeness, CIE values for $Ca_3Y_{1.98}Tb_{0.02}Si_3O_{12}$ and $Ca_3Y_{1.98}Eu_{0.02}Si_3O_{12}$ are also included in both diagram and table. In this case, control over the doping ratio allows obtaining a final emission colour that varies from pinkish-white to yellowish-white in the co-doped materials.

#258303 Received 26 Jan 2016; revised 11 Apr 2016; accepted 11 Apr 2016; published 28 Apr 2016

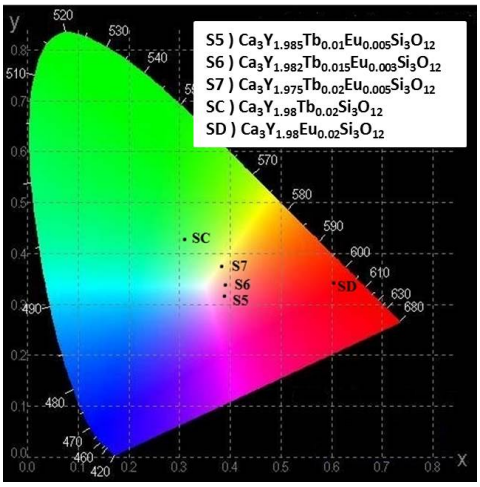

Fig. 6. CIE diagram coordinates of $Ca_3Y_{1.98}Tb_{0.02}Si_3O_{12}$, $Ca_3Y_{1.98}Tb_{0.02}Si_3O_{12}$ and $Ca_3Y_{2-x-y}Tb_xEu_ySi_3O_{12}$ excited at 377, 378 and 393 nm respectively.

Table 4. Calculated values for CIE coordinates of $Ca_3Y_{1.98}Tb_{0.02}Si_3O_{12}$ and $Ca_3Y_{2-x-y}Tb_xEu_ySi_3O_{12}$ excited at 378 nm and $Ca_3Y_{1.98}Eu_{0.02}Si_3O_{12}$ excited at 393 nm.

Material	x	y
$Ca_3Y_{1.98}Tb_{0.02}Si_3O_{12}$	0.3164	0.4351
$Ca_3Y_{1.98}Eu_{0.02}Si_3O_{12}$	0.6007	0.3495
$Ca_3Y_{1.975}Tb_{0.02}Eu_{0.005}Si_3O_{12}$	0.3856	0.3751
$Ca_3Y_{1.982}Tb_{0.015}Eu_{0.003}Si_3O_{12}$	0.3900	0.3409
$Ca_3Y_{1.985}Tb_{0.01}Eu_{0.005}Si_3O_{12}$	0.3891	0.3203

The excitation spectra present no significant differences with the ones measured for the gadolinium-based materials. Also in this case, no evidence of Tb^{3+}-Eu^{3+} energy transfer process has been found. The same considerations made for the gadolinium phosphors apply here.

Decay curves for Tb^{3+} and Eu^{3+} emission were measured upon excitation at 378 nm. The obtained time constants are reported in Table 5. In the co-doped phosphors there is a clear rise at short times in the decay curves for Tb^{3+} emission from $^5D_4$, as observed in the gadolinium samples, and the decay constant is also much longer than in concentrated Tb^{3+} systems. Since in these compounds the Tb^{3+} concentration is also low, all the considerations discussed in the case of the gadolinium host apply in this case. The decay curves for Tb^{3+} emission from $^5D_3$ have been also measured. As observed previously for the gadolinium phosphors, curves are not exponential and the decay constant is about 1 ms. Again, and due to the low levels of doping, decay constant is not affected by Eu^{3+} concentration (not for blue or green emission).

Regarding decay curves for Eu^{3+} $^5D_0$ emission for the co-doped samples, the curves are also well fitted by a single exponential function, and the time constants calculated from them are similar to the obtained for the gadolinium phosphors. The values are reported in Table 5. As well as it was observed before, there are no significant changes when varying Eu^{3+} concentration.

Table 5. Decay data for the luminescent levels of Tb^{3+} and Eu^{3+} in several yttrium hosts upon UV excitation.

Material	Excited state	Decay time (ms)	Excited state	Decay time (ms)
$Ca_3Y_{1.98}Tb_{0.02}Si_3O_{12}$	$^5D_4$ (Tb^{3+})	2.28 rise + decay	--	--
$Ca_3Y_{1.98}Eu_{0.02}Si_3O_{12}$	--	--	$^5D_0$ (Eu^{3+})	1.88
$Ca_3Y_{1.94}Tb_{0.02}Eu_{0.05}Si_3O_{12}$	$^5D_4$ (Tb^{3+})	2.23 rise + decay	$^5D_0$ (Eu^{3+})	1.87
$Ca_3Y_{1.97}Tb_{0.015}Eu_{0.003}Si_3O_{12}$	$^5D_4$ (Tb^{3+})	2.25 rise + decay	$^5D_0$ (Eu^{3+})	1.85
$Ca_3Y_{1.98}Tb_{0.01}Eu_{0.05}Si_3O_{12}$	$^5D_4$ (Tb^{3+})	2.29 rise + decay	$^5D_0$ (Eu^{3+})	1.85

#258303 Received 26 Jan 2016; revised 11 Apr 2016; accepted 11 Apr 2016; published 28 Apr 2016

4. Conclusions

In this work the luminescence spectra and decay curves of several $Ca_3Gd_{2-x-y}Tb_xEu_ySi_3O_{12}$ and $Ca_3Y_{2-x-y}Tb_xEu_ySi_3O_{12}$ powders have been systematically studied. Experiments for various Tb^{3+} and Eu^{3+} doping, and co-doping concentration have been performed. The obtained results indicate that the $^5D_4$ level can be populated from $^5D_3$ via a multiphonon relaxation process, while $^5D_3$-$^5D_4$ cross relaxation does not pay a relevant role. Therefore, in this case quenching of blue emission is avoided. No evidence of Tb^{3+}-Eu^{3+} energy transfer process has been found in any of the co-doped systems as a result of the low doping levels, that do not favour the Tb^{3+}-Tb^{3+} energy migration, nor direct Tb^{3+}-Eu^{3+} transfer. The obtained results show that for the present samples the emission colour strongly depends on the Tb-Eu ratio, and not on the total doping concentration of each ion. Controlling the doping ratio leads to close-to-white emission in various silico-carnotite compounds, opening an interesting opportunity in the search for novel phosphors for white-LED excited in the UV.

Acknowledgments

We would like to thank the European Commission for funding through the Marie Curie Initial Training network LUMINET, grant agreement No. 316906. Expert technical assistance by Erica Viviani is gratefully acknowledged.

#258303 Received 26 Jan 2016; revised 11 Apr 2016; accepted 11 Apr 2016; published 28 Apr 2016